Report

Current Biology

Co-polymers of Actin and Tropomyosin Account for a Major Fraction of the Human Actin Cytoskeleton

Graphical Abstract

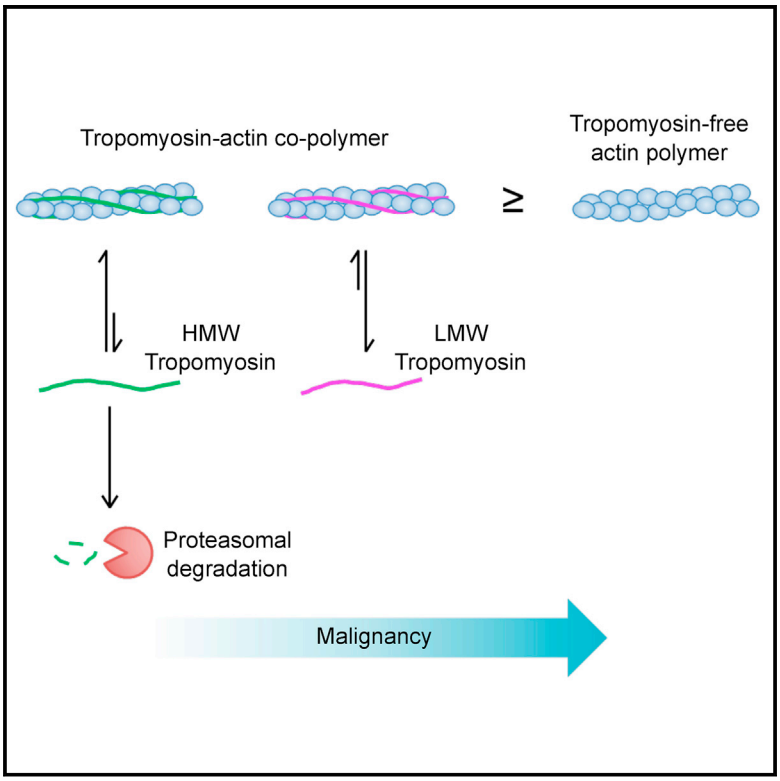

Authors

Joyce C.M. Meiring, Nicole S. Bryce, Yao Wang, ..., Jeffrey Stear, Edna C. Hardeman, Peter W. Gunning

Correspondence

p.gunning@unsw.edu.au

In Brief

Meiring et al. find that tropomyosin is present in saturating levels in human cells and that actin-tropomyosin co-polymers make up a major fraction of the actin cytoskeleton.

Highlights

- Tropomyosin is present in saturating concentrations in human cells
- Cell transformation reduces the fraction of tropomyosin-associated actin filaments
- Unlike LMW tropomyosins, HMW isoforms are primarily co-polymerized with actin
- HMW tropomyosins are more susceptible to proteasomal degradation than LMW isoforms

Meiring et al., 2018, Current Biology *28*, 1–7
July 23, 2018
https://doi.org/10.1016/j.cub.2018.05.053

CellPress

Please cite this article in press as: Meiring et al., Co-polymers of Actin and Tropomyosin Account for a Major Fraction of the Human Actin Cytoskeleton, Current Biology (2018), https://doi.org/10.1016/j.cub.2018.05.053

Current Biology
Report

Co-polymers of Actin and Tropomyosin Account for a Major Fraction of the Human Actin Cytoskeleton

Joyce C.M. Meiring,[1] Nicole S. Bryce,[1] Yao Wang,[1] Manuel H. Taft,[2,3] Dietmar J. Manstein,[2,3] Sydney Liu Lau,[4] Jeffrey Stear,[1] Edna C. Hardeman,[1] and Peter W. Gunning[1,5,*]
[1]Cellular and Genetic Medicine Unit, School of Medical Sciences, University of New South Wales, Sydney, NSW 2052, Australia
[2]Institute for Biophysical Chemistry, Medizinische Hochschule Hannover, Hannover 30625, Germany
[3]Division for Structural Biochemistry, Medizinische Hochschule Hannover, Hannover 30625, Germany
[4]Bioanalytical Mass Spectrometry Facility, Mark Wainwright Analytical Centre, University of New South Wales, Sydney, NSW 2052, Australia
[5]Lead Contact
*Correspondence: p.gunning@unsw.edu.au
https://doi.org/10.1016/j.cub.2018.05.053

SUMMARY

Tropomyosin proteins form stable coiled-coil dimers that polymerize along the α-helical groove of actin filaments [1]. The actin cytoskeleton consists of both co-polymers of actin and tropomyosin and polymers of tropomyosin-free actin [2]. The fundamental distinction between these two types of filaments is that tropomyosin determines the functional capability of actin filaments in an isoform-dependent manner [3–9]. However, it is unknown what portion of actin filaments are associated with tropomyosin. To address this deficit, we have measured the relative distribution between these two filament populations by quantifying tropomyosin and actin levels in a variety of human cell types, including bone (U2OS); breast epithelial (MCF-10A); transformed breast epithelial (MCF-7); and primary (BJpar), immortalized (BJeH), and Ras-transformed (BJeLR) BJ fibroblasts [10]. Our measurements of tropomyosin and actin predict the saturation of the actin cytoskeleton, implying that tropomyosin binding must be inhibited in order to generate tropomyosin-free actin filaments. We find the majority of actin filaments to be associated with tropomyosin in four of the six cell lines tested and the portion of actin filaments associated with tropomyosin to decrease with transformation. We also discover that high-molecular-weight (HMW), unlike low-molecular-weight (LMW), tropomyosin isoforms are primarily co-polymerized with actin in untransformed cells. This differential partitioning of tropomyosins is not due to a lack of N-terminal acetylation of LMW tropomyosins, but it is, in part, explained by the susceptibility of soluble HMW tropomyosins to proteasomal degradation. We conclude that actin-tropomyosin co-polymers make up a major fraction of the human actin cytoskeleton.

RESULTS AND DISCUSSION

Tropomyosin Co-localizes with Most Actin Structures

Tropomyosins have been implicated in a variety of different actin structures, including stress fibers [6], lamellipodia [7], granules [11], endosomes [12], cortical actin [13], the epithelial zonula adherens [14], podosomes [15], the cleavage furrow of dividing cells [16, 17], mitotic spindles [16], actin ruffles [18], short microfilaments associated with the Golgi [16, 19], filopodia [8], and the endoplasmic reticulum [20]. Mammalian cells can produce over 40 different splice variants using four different tropomyosin genes, TPM1–4, and the resulting gene products can be divided into low-molecular-weight (LMW) isoforms that span six actin monomers and high-molecular-weight (HMW) isoforms that span seven actin monomers.

Using a panel of antibodies to different tropomyosin isoforms, since no single tropomyosin antibody detects all isoforms, we find that subgroups of tropomyosin isoforms co-localize with almost all actin cables in BJpar cells (Figures S1A–S1C, solid arrows). Rare regions of actin cables were detected that do not stain with one of the antibodies (Figures S1A–S1C, open arrows); however, it is possible that other tropomyosin isoforms are associated with those filaments. Similar observations were made in immunostained BJeH, U2OS, and MCF-10A cells (Figure 1). BJeLR cells show a distinct loss of actin cables but retain some finer actin structures that co-localize with various tropomyosins (Figure 1). MCF-7 cells do not produce stress fibers either; rather, the most prominent actin structure in these cells is a contractile actin ring that was observed to co-localize with Tpm3.1/3.2 and Tpm4.2, but not Tpm1.6/1.7/2.1/4.1 (Figure 1). Actin cables consist of numerous actin filaments, and confocal imaging does not allow for quantitation of how many individual actin filaments exist as either actin polymer alone or actin polymer associated with tropomyosin. Hence, we have addressed this question using a biochemical approach.

Tropomyosin Quantification

Two tropomyosin polymers run in parallel along an actin filament, one in each major actin groove [1]. *In vitro* studies have demonstrated that the interaction between actin and individual tropomyosin dimers is quite weak; however, end-to-end-linked

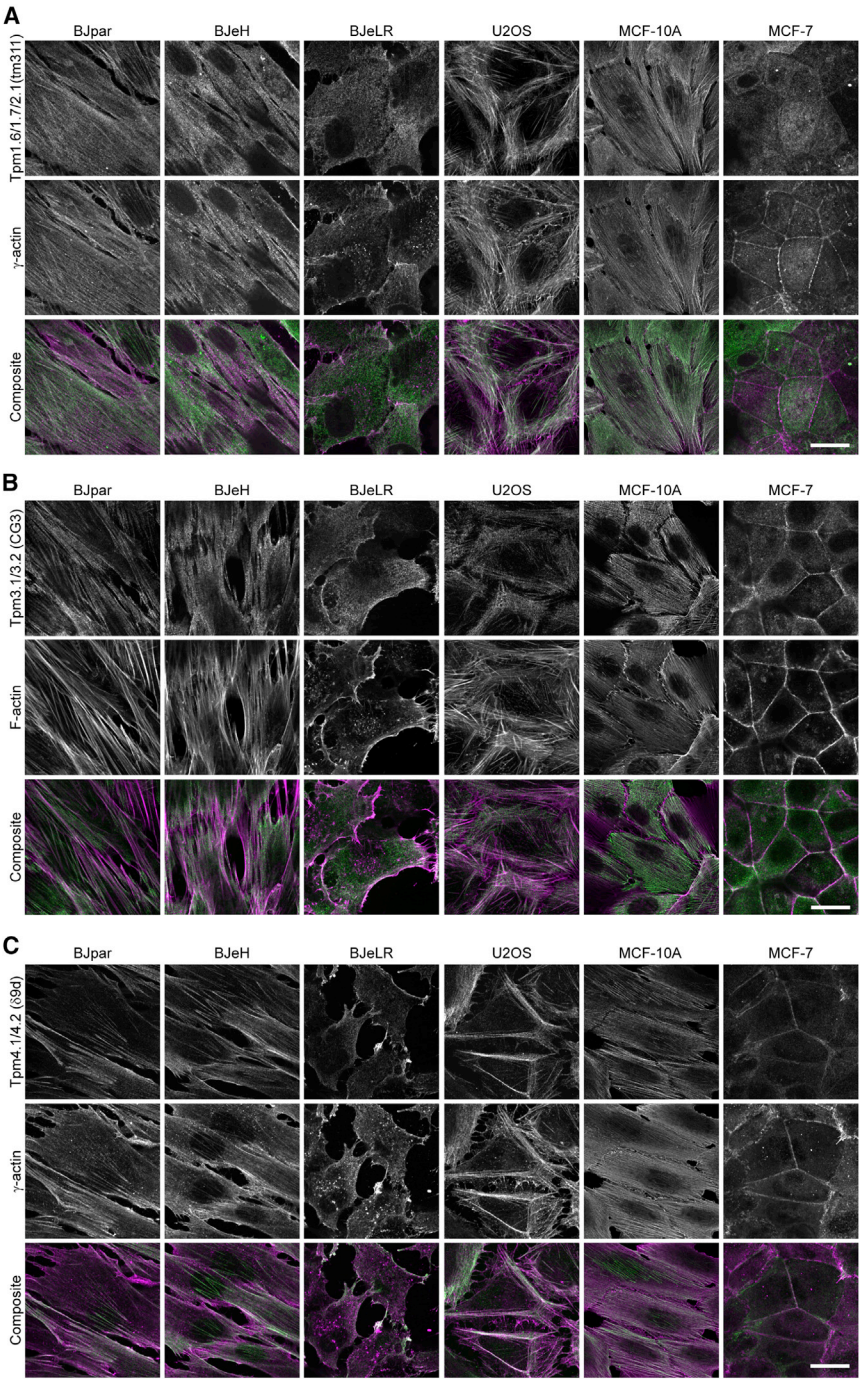

Figure 1. Most Actin Structures Co-localize with Tropomyosin in BJpar, BJeH, BJeLR, U2OS, MCF-10A, and MCF-7 Cells

(A–C) Cells were immunostained against (A) Tpm1.6/1.7/2.1/4.1, (B) Tpm3.1/3.2, or (C) Tpm4.1/4.2 (green) and co-stained with γ-actin (A and C) or phalloidin (B) (magenta); overlap in composite images is shown in white. Scale bar, 20 μm. See also Figure S1.

tropomyosins bind to actin filaments with approximately 1,000-fold greater affinity, promoting the uniform coating of actin filaments [21]. To determine whether our cell lines produce sufficient tropomyosin to be able to saturate all the individual actin filaments, the quantities of the major tropomyosin isoforms and actin were measured in moles per gram of total protein, to allow for the evaluation of the molar ratio of actin to tropomyosin. The quantification was performed through the use of a set of actin and recombinant tropomyosin protein standards and a panel of anti-tropomyosin antibodies that detect the full spectrum of tropomyosin isoforms [22] (Figure S2). G-actin-to-F-actin ratios were measured and combined with our total actin quantification to calculate the amount of actin in the form of G-actin or F-actin in moles per gram of total protein. Based on the number of actin monomers that could be bound by each tropomyosin (6 actin monomers per LMW tropomyosin dimer and 7 actin monomers per HMW tropomyosin dimer) and the molar ratio of tropomyosins to actin, we calculated that there is more than sufficient tropomyosin to coat all of the actin polymers in all six cell types (Table 1). This excess of tropomyosin may be important for establishing a protein equilibrium that is conducive to the interaction of tropomyosin with actin. The majority of other actin-binding proteins have not yet been quantified in cells, so it is possible that there are others also present at saturating concentrations; however, the actin-binding proteins that have been quantified in mammalian cells, ADF/Cofilin, profilin, gelsolin, CapZ, Arp2, and Arp3, were all found to be expressed at low levels relative to that of actin [23].

As is typically observed in transformed cells [24–26], BJeLR cells showed a dramatic decrease in the expression of all tropomyosin isoforms, especially the HMW isoforms (Tpm1.6/1.7 and Tpm2.1/4.1), compared to the primary and immortalized fibroblasts. The exception to this observation was Tpm3.1/3.2, which exhibited an increase in expression (Table 1). In BJeLR cells, about 70% of the total tropomyosin consisted of Tpm3.1/3.2. The majority of the additional tropomyosin was composed of the other LMW tropomyosins, Tpm1.8/1.9 and Tpm4.2 (Table 1). Similar to the BJeLR cells, U2OS, MCF-10A, and MCF-7 cells also expressed relatively low levels of HMW tropomyosin isoforms, and Tpm3.1/3.2 also made up the majority of the tropomyosin in these cells (Table 1). This result may reflect the requirement in transformed cells for Tpm3.1/3.2 filaments in MAPK/ERK signaling [27], glucose transport [13], and the inhibition of apoptosis [28]. This result was expected for the U2OS and MCF-7 cells as these cell lines were known to be transformed,

Table 1. Quantity of Tropomyosin and Actin in Human Cells Indicates an Excess of Tropomyosin Required to Saturate All Actin Filaments

	Protein (nmol/g Total Cell Protein ± SD)					
	BJpar	BJeH	BJeLR	U2OS	MCF-10A	MCF-7
Tpm1.6/1.7	83 ± 3	100 ± 16	11 ± 1	18 ± 3	14 ± 4	10 ± 2
Tpm1.8/1.9	127 ± 8	109 ± 17	27 ± 19	22 ± 4	7 ± 1	78 ± 22
Tpm2.1/4.1	27 ± 1	18 ± 4	6 ± 1	2.5 ± 0.1	16 ± 1	<1
Tpm3.1/3.2	150 ± 22	176 ± 3	260 ± 29	64 ± 11	154 ± 13	115 ± 23
Tpm4.2	216 ± 13	223 ± 55	66 ± 12	18 ± 11	12 ± 1	13 ± 3
Total Tpm	603	626	370	124	203	216
G-actin	918 ± 206	719 ± 375	310 ± 27	186 ± 34	568 ± 149	650 ± 115
F-actin	809 ± 183	650 ± 340	207 ± 22	148 ± 28	560 ± 148	460 ± 85
Percentage of F-actin that could be saturated by tropomyosin	230%	298%	541%	259%	112%	143%

See also Figure S2 and Tables S1–S3.

but not for the MCF-10A cell line that is typically used as a model for normal human mammary epithelial cells. However, a recent study of MCF-10A cells revealed unique and atypical differentiation marker expression, calling into question their suitability as a model of normal mammary cells [29].

The observation that tropomyosins are present at high enough levels to saturate the actin cytoskeleton mole for mole led us to quantify how much of the actin cytoskeleton could be saturated based on tropomyosin-binding affinities. To this end, we estimated the concentration of actin and tropomyosin in cells based on our quantification and previous reports that cells contain approximately 200 g protein per 1 L volume [30, 31] (Table S1). We used these concentration estimates together with tropomyosin Hill coefficients and experimental $K_{d(app)}/K_{50\%}$ values from the literature [4, 32] to calculate the predicted binding capacity of each tropomyosin in these cells, without accounting for binding competition or binding catalysts (Table S2). In all 6 cell lines, all tropomyosins, except for un-acetylated Tpm2.1, were predicted to be almost completely bound to actin filaments. This observation predicts that the generation of tropomyosin-free actin filaments would, of necessity, require the active inhibition of tropomyosin binding to filaments. Some actin-binding proteins known to compete with tropomyosin include cofilin, fimbrin, and α-actinin [9, 33] as well as Arp2/3-branched actin networks, which are incompatible with tropomyosin binding [34]. Conversely, mediators of tropomyosin recruitment like formins [6, 35] and a subset of myosins [5, 36, 37] are expected to favor the binding to actin of specific tropomyosin isoforms.

Partitioning of Tropomyosins to F-actin-Associated versus Soluble Pools

Since there is insufficient actin in these cells to accommodate the predicted binding of all the tropomyosins to actin filaments, we measured what portion of tropomyosin was associating with actin filaments. This was done by quantifying the partitioning of the different tropomyosin isoforms between the insoluble (F-actin) and the soluble (G-actin) fractions. In the BJpar, BJeH, and MCF-10A cells, the HMW tropomyosins (1.6/1.7 and 2.1/4.1) were largely found in the insoluble fraction, whereas the majority of the LMW Tpms (1.8/1.9, 3.1/3.2, and 4.2) were found in the soluble fraction (Figures 2A, 2B, 2E, and 2G). This result was not predicted from the binding calculations (Table S2) but may reflect the greater binding cooperativity [4] and stability of binding [9] of HMW, compared with LMW, tropomyosins observed in *in vitro* cell-free analyses. The high soluble levels of Tpm3.1/3.2 may explain the rapid exchange of soluble Tpm3.1 with Tpm3.1-containing actin filaments observed in cell-free assays [9], cells in culture, and intravital imaging in mice [39]. Soluble tropomyosin itself may also play a role in regulating the actin cytoskeleton, such as inhibiting gelsolin-mediated actin severing [40].

Furthermore, the preferential sorting of Tpm2.1 to the pellet suggests that the majority of Tpm2.1 is most likely acetylated, since acetylated Tpm2.1 has a much higher affinity for actin filaments than the un-acetylated form [32], and based on our calculations un-acetylated Tpm2.1 could not achieve this extent of partitioning (Table S2). The high level of soluble Tpm3.1/3.2 and Tpm4.2 is not due to a lack of acetylation. We measured the prevalence of acetylated tropomyosin and found that all detected Tpm4.2 and Tpm3.1/3.2 was N-terminally acetylated (Table S3). Unfortunately, we have been unable to detect the N terminus of the other isoforms using multiple approaches.

In contrast with BJpar, BJeH, and MCF-10A cells, the partitioning of tropomyosin isoforms to the actin-bound fraction is substantially reduced in the transformed cell lines (BJeLR, U2OS, and MCF-7; Figures 2C, 2D, 2F, and 2G), suggesting that tropomyosin association with actin filaments is inhibited in these cells compared with untransformed cells. Only Tpm1.6/1.7 exhibits enrichment in the pellet fraction, but the levels are still reduced in comparison with that observed in primary and immortalized cells (Figure 2G). We also observed an extra band under Tpm1.8 in the F-actin fraction, exclusive to the mammary epithelial cells (MCF-7 and MCF-10A), which we identified as Tpm1.9 (Figure 2G) [38].

We calculated the population of actin filaments saturated with tropomyosin by first multiplying the insoluble:soluble ratio of each tropomyosin (Figure 2G) with the amount of each tropomyosin present in each cell type (Table 1) to estimate the amount of tropomyosin present in the actin filament pellet. These values

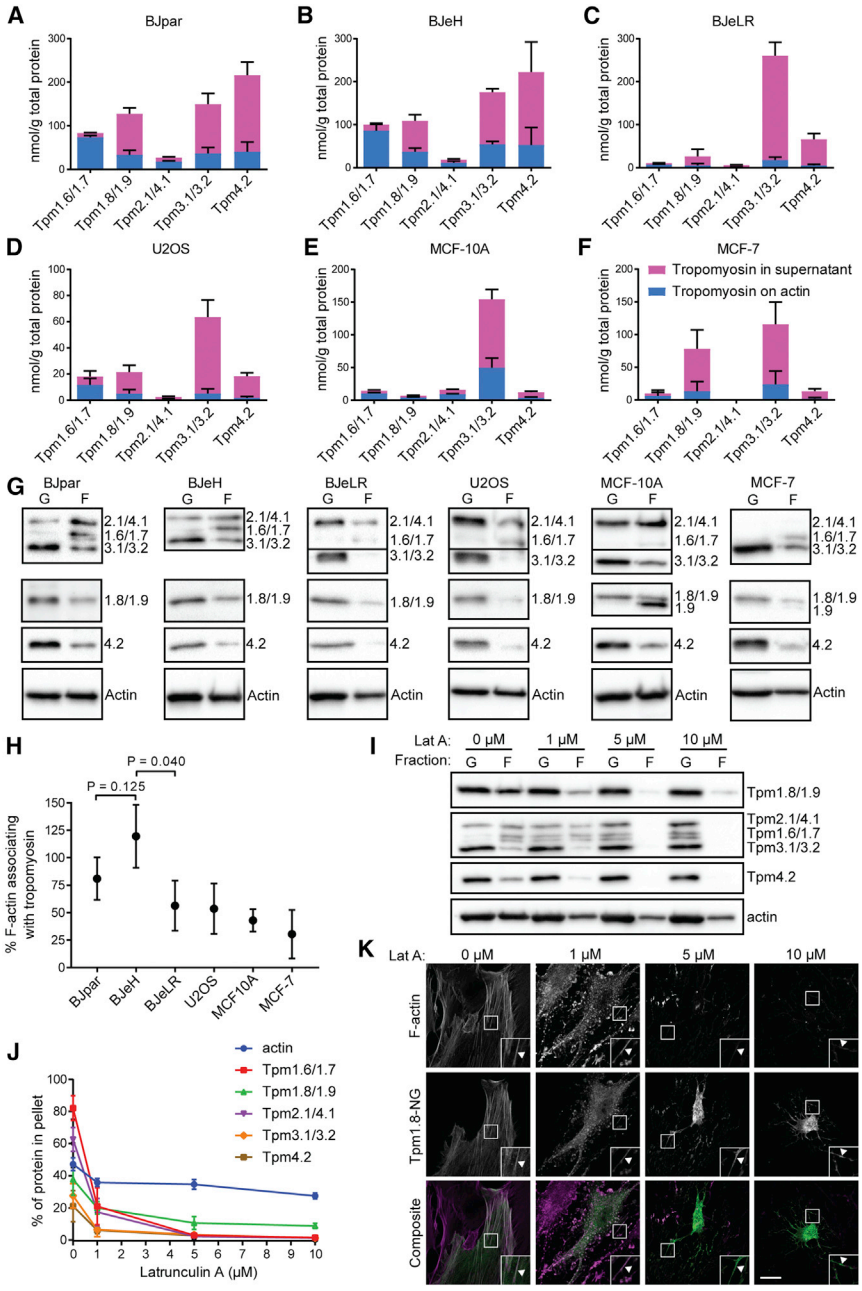

Figure 2. Tropomyosin Partitioning between Soluble and Insoluble Pools

(A–F) Quantity of tropomyosin in soluble and insoluble pools in (A) BJpar, (B) BJeH, (C) BJeLR, (D) U2OS, (E) MCF-10A, and (F) MCF-7 cells.

(G) Blots showing tropomyosin and actin partitioning in all six cell lines. Tpm1.9 runs slightly faster than Tpm1.8 in the insoluble fraction due to fractionated protein pellets being resuspended in urea [38], as seen in MCF-10A and MCF-7 cell lines. G, soluble; F, insoluble.

(H) Estimated population of actin filaments associated with tropomyosin was calculated based on total cellular tropomyosin and actin quantities and the portion of actin and tropomyosin in the insoluble pool of all six cell lines. As a control experiment, BJeH cells were pre-treated with 0, 1, 5, or 10 μM Lat A for 1 hr prior to fractionation.

(I and J) Blots (I) and graph (J) based on results from 3 independent experiments demonstrate that tropomyosin pelleting is proportional to actin cytoskeleton integrity. The only tropomyosin that pellets with F-actin at higher concentrations of Lat A is Tpm1.8/1.9.

(K) Confocal images of BJeH cells transfected with Tpm1.8-NeonGreen (Tpm1.8-NG, green), treated with 0, 1, 5, or 10 μM Lat A for 1 hr, and stained with ATTO 647n-conjugated phalloidin (magenta) show that Tpm1.8-NG co-localizes with F-actin at all tested concentrations of Lat A (arrows). All graphs show data presented as mean ± SD. Scale bar, 20 μm. See also Figure S3.

were multiplied by the actin-binding capacity (actin-binding sites per tropomyosin dimer) of each tropomyosin isoform then summed for each cell type and compared with the amount of actin filament in each cell type to yield the fraction of actin filaments saturated by tropomyosin (Figure 2H). There was a diverse spread across the different cell lines, with >80% of actin filaments estimated to be associated with tropomyosin for the BJpar and BJeH cell lines and 30%–60% estimated for the transformed cell lines and the MCF-10A cells (Figure 2H). The BJeLR estimate was found to be significantly smaller than its untransformed BJeH counterpart (Figure 2H). In 4 (BJpar, BJeH, BJeLR, and U2OS) of the 6 cell lines tested, more than half of the actin filaments were estimated to be saturated with tropomyosin (Figure 2H), suggesting that tropomyosin-associated actin filaments make up a major component of the human actin cytoskeleton.

It was predicted the majority of actin filaments would be associated with tropomyosin, given that tropomyosins localize to most actin structures, are important for stabilizing actin filaments, and support the function of myosin motors [5, 6, 41–43]. We conclude that levels of tropomyosin-associated actin filaments in cells are not simply a product of the concentration of free tropomyosin but that the production of different filament types is actively regulated by the cell. Our data also demonstrate that the presence of actin bundles alone does not necessarily determine the fraction of tropomyosin-actin polymer in a cell, since we observed that BJeLR cells, which do not contain actin bundles, and U2OS cells, which contain prominent actin bundles, both have similar levels of tropomyosin saturation of their actin cytoskeleton (Figures 1 and 2H).

To confirm that the co-sedimentation of tropomyosin with actin filaments in our partitioning assay was a result of tropomyosin interacting with actin filaments, we performed a control experiment perturbing the actin cytoskeleton in BJeH cells with various concentrations of Latrunculin A (Lat A) (Figures 2I–2K). Lat A does not interact with actin filaments to cause depolymerization; rather, it binds to monomeric actin and inhibits

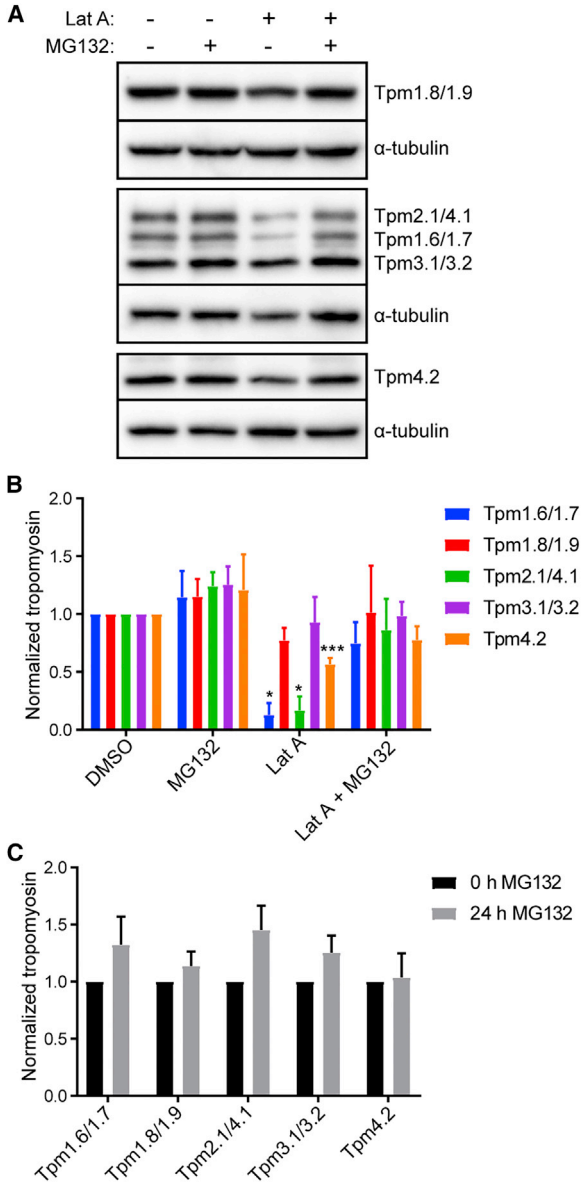

Figure 3. High-Molecular-Weight Tropomyosin Isoforms Are Degraded by the Proteosome When Excluded from Actin Filaments

BJpar cells were treated with DMSO or Lat A with or without MG132 for 6 hr and blotted for tropomyosin, with α-tubulin as a loading control.

(A and B) Representative blots (A) and graph (B) based on 4 experimental replicates show a large decrease in HMW tropomyosin isoforms (Tpm1.6/1.7 and Tpm2.1/4.1) and a small decrease in Tpm4.2 levels with Lat A treatment, which could be ameliorated with the addition of proteosome inhibitor MG132.

(C) BJpar cells were treated with proteosome inhibitor MG132 or DMSO control for 24 hr, and tropomyosin levels were measured and normalized to the DMSO control. Graph shows results from 3 independent experiments, where no significant changes in tropomyosin levels were observed. All graphs show data presented as mean ± SD.*$p < 0.05$ and ***$p < 0.001$.

the incorporation of the bound actin into growing actin filaments [44]. Hence, in the presence of Lat A, actin filaments as they turn over release actin monomer and associated proteins, including tropomyosin, and the rate of reassembly of actin filaments is inhibited by the binding of Lat A to the actin monomer pool. This leads to severely disorganized actin filaments, which often appear as aggregates (Figures 2K and S3), as seen in many cell biology studies [45, 46]. Tropomyosin does not co-pellet with the resulting newly synthesized disorganized filaments, with the exception of a reduced quantity of Tpm1.8/1.9 (Figures 2I and 2J), which suggests that, when the rate of actin polymerization is compromised, tropomyosin co-polymerization is largely abrogated. This finding is consistent with tropomyosin co-polymerizing with actin and further suggests that tropomyosin cannot bind to actin filament aggregates. It also confirms that the co-pelleting of tropomyosin with actin filaments is indeed actin filament dependent. Furthermore, fluorescently tagged Tpm1.8 continues to co-localize with actin filaments at different concentrations of Lat A (arrows, Figure 2K), while Tpm3.1/3.2 co-localizes very poorly with F-actin after treatment with 5 or 10 μM Lat A (arrows, Figure S3). This result may reflect the recent finding that Tpm1.8/1.9 is the only isoform known to localize at the leading edge of cells and is capable of coating newly de-branched actin filaments [7], as well as its high actin-binding affinity observed *in vitro* [5].

HMW Tropomyosins Are Degraded by the Proteasome When Excluded from Actin Filaments

Lat A treatment discriminates the relative stability of HMW and LMW tropomyosins. While short-term (≤1-hr) Lat A treatments did not significantly impact total tropomyosin levels, we found that long-term (6-hr) Lat A treatment resulted in an 83%–92% reduction of HMW tropomyosins and a 43% reduction in Tpm4.2 that could be ameliorated with the addition of proteasome inhibitor MG132 (Figures 3A and 3B). Taken together with our data that show that Lat A perturbs actin structures in BJ fibroblasts and disrupts actin-tropomyosin co-polymers (Figures 2I–2K), this result suggests that HMW tropomyosins are preferentially degraded when they are not associated with actin filaments. This most likely reflects the observation that HMW tropomyosins have a lower stability than LMW tropomyosins [47] and may also help to explain the loss of HMW isoforms in transformed cells. The HMW tropomyosin isoforms may be degraded in transformed cells as a result of failure to be incorporated into actin filaments, which we observed, as HMW tropomyosin partitioning with actin filaments was indeed reduced in transformed cells (Figure 2G). Degradation of HMW isoforms such as Tpm2.1 is also predicted to reduce the cell's sensitivity to apoptosis [28] and enable cells to engage in anchorage-independent growth [48] and to form contractile focal contacts [42], thus promoting a transformed cell phenotype.

The turnover of HMW tropomyosins by the proteasome raises the question of how rapidly they are turning over in untreated cells. Exposure of primary BJ fibroblasts to MG132 for 24 hr resulted in no significant increase in tropomyosin levels (Figure 3C). We therefore suggest that there is not extensive turnover of the HMW tropomyosin mediated by the proteasome under normal growth conditions.

We conclude that tropomyosins (1) localize to most actin structures in cultured cells, (2) associate with the majority of actin filaments in untransformed cultured cells, (3) are present in sufficient levels to saturate all actin filaments and (4) would therefore need to be actively inhibited from binding to actin filaments to allow the formation of tropomyosin-free actin filaments, and

(5) are inhibited from binding actin filaments in transformed cells, as well as that (6) LMW isoforms are mostly soluble and display reduced susceptibility to proteolytic degradation and (7) HMW isoforms are mostly actin bound and show increased susceptibility to degradation by the proteasome in their soluble form. These results indicate that co-polymers of actin with tropomyosin make up a major fraction of actin filaments in human cells. Since tropomyosins determine the functional and kinetic properties of actin filaments [4, 9] and the functional consequences of their engagement with myosin motors [3, 5, 9, 42, 43], our results highlight the importance of identifying what type of actin filament is engaged in any specific cellular function.

STAR★METHODS

Detailed methods are provided in the online version of this paper and include the following:

- KEY RESOURCES TABLE
- CONTACT FOR REAGENT AND RESOURCE SHARING
- EXPERIMENTAL MODEL AND SUBJECT DETAILS
  - Cell culture
- METHOD DETAILS
  - Cell transfection
  - Immunofluorescence microscopy
  - Antibodies and staining
  - Actin and tropomyosin quantification
  - Tropomyosin partitioning assay
  - Liquid chromatography (LC)
  - Tandem mass spectrometry (MS/MS)
  - Drug treatments
- QUANTIFICATION AND STATISTICAL ANALYSIS

SUPPLEMENTAL INFORMATION

Supplemental Information includes three figures and three tables and can be found with this article online at https://doi.org/10.1016/j.cub.2018.05.053.

ACKNOWLEDGMENTS

We would like to thank Galina Schevzov and Vera Dugina for helpful discussions and the Australian National Health and Medical Research Council (NHMRC), the Kids Cancer Project, and the Deutsche Forschungsgemeinschaft (DFG) for supporting this work.

AUTHOR CONTRIBUTIONS

Conceptualization, J.C.M.M. and P.W.G.; Data Acquisition, J.C.M.M. and Y.W.; Mass Spectrometry, S.L.L.; Data Analysis, J.C.M.M. and M.H.T.; Drafting of Manuscript, J.C.M.M.; Reviewing of Manuscript, P.W.G., N.S.B., J.S., E.C.H., D.J.M., and M.H.T.; Funding Acquisition and Supervision, N.S.B., D.J.M., P.W.G., and E.C.H.

DECLARATION OF INTERESTS

P.W.G. is a member of the Scientific Advisory Board of Kazia, a company that is commercializing anti-tropomyosin drugs for the treatment of cancer, and his lab receives funding from Kazia to evaluate anti-tropomyosin drug candidates.

Received: December 5, 2017
Revised: April 20, 2018
Accepted: May 17, 2018
Published: July 5, 2018

REFERENCES

1. Li, X.E., Tobacman, L.S., Mun, J.Y., Craig, R., Fischer, S., and Lehman, W. (2011). Tropomyosin position on F-actin revealed by EM reconstruction and computational chemistry. Biophys. J. *100*, 1005–1013.
2. Lazarides, E. (1976). Two general classes of cytoplasmic actin filaments in tissue culture cells: the role of tropomyosin. J. Supramol. Struct. *5*, 531(383)–563(415).
3. Bryce, N.S., Schevzov, G., Ferguson, V., Percival, J.M., Lin, J.J., Matsumura, F., Bamburg, J.R., Jeffrey, P.L., Hardeman, E.C., Gunning, P., and Weinberger, R.P. (2003). Specification of actin filament function and molecular composition by tropomyosin isoforms. Mol. Biol. Cell *14*, 1002–1016.
4. Janco, M., Bonello, T.T., Byun, A., Coster, A.C., Lebhar, H., Dedova, I., Gunning, P.W., and Böcking, T. (2016). The impact of tropomyosins on actin filament assembly is isoform specific. Bioarchitecture *6*, 61–75.
5. Pathan-Chhatbar, S., Taft, M.H., Reindl, T., Hundt, N., Latham, S.L., and Manstein, D.J. (2018). Three mammalian tropomyosin isoforms have different regulatory effects on nonmuscle myosin-2B and filamentous β-actin *in vitro*. J. Biol. Chem. *293*, 863–875.
6. Tojkander, S., Gateva, G., Schevzov, G., Hotulainen, P., Naumanen, P., Martin, C., Gunning, P.W., and Lappalainen, P. (2011). A molecular pathway for myosin II recruitment to stress fibers. Curr. Biol. *21*, 539–550.
7. Brayford, S., Bryce, N.S., Schevzov, G., Haynes, E.M., Bear, J.E., Hardeman, E.C., and Gunning, P.W. (2016). Tropomyosin Promotes Lamellipodial Persistence by Collaborating with Arp2/3 at the Leading Edge. Curr. Biol. *26*, 1312–1318.
8. Creed, S.J., Desouza, M., Bamburg, J.R., Gunning, P., and Stehn, J. (2011). Tropomyosin isoform 3 promotes the formation of filopodia by regulating the recruitment of actin-binding proteins to actin filaments. Exp. Cell Res. *317*, 249–261.
9. Gateva, G., Kremneva, E., Reindl, T., Kotila, T., Kogan, K., Gressin, L., Gunning, P.W., Manstein, D.J., Michelot, A., and Lappalainen, P. (2017). Tropomyosin Isoforms Specify Functionally Distinct Actin Filament Populations In Vitro. Curr. Biol. *27*, 705–713.
10. Hahn, W.C., Counter, C.M., Lundberg, A.S., Beijersbergen, R.L., Brooks, M.W., and Weinberg, R.A. (1999). Creation of human tumour cells with defined genetic elements. Nature *400*, 464–468.
11. Masedunskas, A., Appaduray, M.A., Lucas, C.A., Lastra Cagigas, M., Heydecker, M., Holliday, M., Meiring, J.C.M., Hook, J., Kee, A., White, M., et al. (2018). Parallel assembly of actin and tropomyosin, but not myosin II, during *de novo* actin filament formation in live mice. J. Cell Sci. *131*, jcs212654.
12. Gormal, R., Valmas, N., Fath, T., and Meunier, F. (2017). A role for tropomyosins in activity-dependent bulk endocytosis? Mol. Cell. Neurosci. *84*, 112–118.
13. Kee, A.J., Yang, L., Lucas, C.A., Greenberg, M.J., Martel, N., Leong, G.M., Hughes, W.E., Cooney, G.J., James, D.E., Ostap, E.M., et al. (2015). An actin filament population defined by the tropomyosin Tpm3.1 regulates glucose uptake. Traffic *16*, 691–711.
14. Caldwell, B.J., Lucas, C., Kee, A.J., Gaus, K., Gunning, P.W., Hardeman, E.C., Yap, A.S., and Gomez, G.A. (2014). Tropomyosin isoforms support actomyosin biogenesis to generate contractile tension at the epithelial zonula adherens. Cytoskeleton (Hoboken) *71*, 663–676.
15. McMichael, B.K., Kotadiya, P., Singh, T., Holliday, L.S., and Lee, B.S. (2006). Tropomyosin isoforms localize to distinct microfilament populations in osteoclasts. Bone *39*, 694–705.
16. Goins, L.M., and Mullins, R.D. (2015). A novel tropomyosin isoform functions at the mitotic spindle and Golgi in Drosophila. Mol. Biol. Cell *26*, 2491–2504.
17. Hughes, J.A., Cooke-Yarborough, C.M., Chadwick, N.C., Schevzov, G., Arbuckle, S.M., Gunning, P., and Weinberger, R.P. (2003). High-molecular-weight tropomyosins localize to the contractile rings of dividing CNS cells but are absent from malignant pediatric and adult CNS tumors. Glia *42*, 25–35.

18. Warren, R.H., Gordon, E., and Azarnia, R. (1985). Tropomyosin in peripheral ruffles of cultured rat kidney cells. Eur. J. Cell Biol. *38*, 245–253.
19. Percival, J.M., Hughes, J.A., Brown, D.L., Schevzov, G., Heimann, K., Vrhovski, B., Bryce, N., Stow, J.L., and Gunning, P.W. (2004). Targeting of a tropomyosin isoform to short microfilaments associated with the Golgi complex. Mol. Biol. Cell *15*, 268–280.
20. Kee, A.J., Bryce, N.S., Yang, L., Polishchuk, E., Schevzov, G., Weigert, R., Polishchuk, R., Gunning, P.W., and Hardeman, E.C. (2017). ER/Golgi trafficking is facilitated by unbranched actin filaments containing Tpm4.2. Cytoskeleton (Hoboken) *74*, 379–389.
21. Schmidt, W.M., Lehman, W., and Moore, J.R. (2015). Direct observation of tropomyosin binding to actin filaments. Cytoskeleton (Hoboken) *72*, 292–303.
22. Schevzov, G., Whittaker, S.P., Fath, T., Lin, J.J., and Gunning, P.W. (2011). Tropomyosin isoforms and reagents. Bioarchitecture *1*, 135–164.
23. dos Remedios, C.G., Chhabra, D., Kekic, M., Dedova, I.V., Tsubakihara, M., Berry, D.A., and Nosworthy, N.J. (2003). Actin binding proteins: regulation of cytoskeletal microfilaments. Physiol. Rev. *83*, 433–473.
24. Matsumura, F., Lin, J.J., Yamashiro-Matsumura, S., Thomas, G.P., and Topp, W.C. (1983). Differential expression of tropomyosin forms in the microfilaments isolated from normal and transformed rat cultured cells. J. Biol. Chem. *258*, 13954–13964.
25. Hendricks, M., and Weintraub, H. (1981). Tropomyosin is decreased in transformed cells. Proc. Natl. Acad. Sci. USA *78*, 5633–5637.
26. Stehn, J.R., Haass, N.K., Bonello, T., Desouza, M., Kottyan, G., Treutlein, H., Zeng, J., Nascimento, P.R., Sequeira, V.B., Butler, T.L., et al. (2013). A novel class of anticancer compounds targets the actin cytoskeleton in tumor cells. Cancer Res. *73*, 5169–5182.
27. Schevzov, G., Kee, A.J., Wang, B., Sequeira, V.B., Hook, J., Coombes, J.D., Lucas, C.A., Stehn, J.R., Musgrove, E.A., Cretu, A., et al. (2015). Regulation of cell proliferation by ERK and signal-dependent nuclear translocation of ERK is dependent on Tm5NM1-containing actin filaments. Mol. Biol. Cell *26*, 2475–2490.
28. Desouza-Armstrong, M., Gunning, P.W., and Stehn, J.R. (2017). Tumor suppressor tropomyosin Tpm2.1 regulates sensitivity to apoptosis beyond anoikis characterized by changes in the levels of intrinsic apoptosis proteins. Cytoskeleton (Hoboken) *74*, 233–248.
29. Qu, Y., Han, B., Yu, Y., Yao, W., Bose, S., Karlan, B.Y., Giuliano, A.E., and Cui, X. (2015). Evaluation of MCF10A as a Reliable Model for Normal Human Mammary Epithelial Cells. PLoS ONE *10*, e0131285.
30. Loewy, A.G., Siekevitz, P., and Open, U. (1969). Cell Structure and Function (Holt, Rinehart and Winston).
31. Fulton, A.B. (1982). How crowded is the cytoplasm? Cell *30*, 345–347.
32. Coulton, A., Lehrer, S.S., and Geeves, M.A. (2006). Functional homodimers and heterodimers of recombinant smooth muscle tropomyosin. Biochemistry *45*, 12853–12858.
33. Christensen, J.R., Hocky, G.M., Homa, K.E., Morganthaler, A.N., Hitchcock-DeGregori, S.E., Voth, G.A., and Kovar, D.R. (2017). Competition between Tropomyosin, Fimbrin, and ADF/Cofilin drives their sorting to distinct actin filament networks. eLife *6*, e23152.
34. Hsiao, J.Y., Goins, L.M., Petek, N.A., and Mullins, R.D. (2015). Arp2/3 complex and cofilin modulate binding of tropomyosin to branched actin networks. Curr. Biol. *25*, 1573–1582.
35. Johnson, M., East, D.A., and Mulvihill, D.P. (2014). Formins determine the functional properties of actin filaments in yeast. Curr. Biol. *24*, 1525–1530.
36. Moraczewska, J. (2002). Structural determinants of cooperativity in actomyosin interactions. Acta Biochim. Pol. *49*, 805–812.
37. Eaton, B.L. (1976). Tropomyosin binding to F-actin induced by myosin heads. Science *192*, 1337–1339.
38. Sung, L.A., Gao, K.M., Yee, L.J., Temm-Grove, C.J., Helfman, D.M., Lin, J.J., and Mehrpouryan, M. (2000). Tropomyosin isoform 5b is expressed in human erythrocytes: implications of tropomodulin-TM5 or tropomodulin-TM5b complexes in the protofilament and hexagonal organization of membrane skeletons. Blood *95*, 1473–1480.
39. Appaduray, M.A., Masedunskas, A., Bryce, N.S., Lucas, C.A., Warren, S.C., Timpson, P., Stear, J.H., Gunning, P.W., and Hardeman, E.C. (2016). Recruitment Kinetics of Tropomyosin Tpm3.1 to Actin Filament Bundles in the Cytoskeleton Is Independent of Actin Filament Kinetics. PLoS ONE *11*, e0168203.
40. Khaitlina, S., Fitz, H., and Hinssen, H. (2013). The interaction of gelsolin with tropomyosin modulates actin dynamics. FEBS J. *280*, 4600–4611.
41. Manstein, D.J., and Mulvihill, D.P. (2016). Tropomyosin-Mediated Regulation of Cytoplasmic Myosins. Traffic *17*, 872–877.
42. Wolfenson, H., Meacci, G., Liu, S., Stachowiak, M.R., Iskratsch, T., Ghassemi, S., Roca-Cusachs, P., O'Shaughnessy, B., Hone, J., and Sheetz, M.P. (2016). Tropomyosin controls sarcomere-like contractions for rigidity sensing and suppressing growth on soft matrices. Nat. Cell Biol. *18*, 33–42.
43. Hundt, N., Steffen, W., Pathan-Chhatbar, S., Taft, M.H., and Manstein, D.J. (2016). Load-dependent modulation of non-muscle myosin-2A function by tropomyosin 4.2. Sci. Rep. *6*, 20554.
44. Morton, W.M., Ayscough, K.R., and McLaughlin, P.J. (2000). Latrunculin alters the actin-monomer subunit interface to prevent polymerization. Nat. Cell Biol. *2*, 376–378.
45. Michael, M., Meiring, J.C.M., Acharya, B.R., Matthews, D.R., Verma, S., Han, S.P., Hill, M.M., Parton, R.G., Gomez, G.A., and Yap, A.S. (2016). Coronin 1B Reorganizes the Architecture of F-Actin Networks for Contractility at Steady-State and Apoptotic Adherens Junctions. Dev. Cell *37*, 58–71.
46. Tang, V.W., and Brieher, W.M. (2012). α-Actinin-4/FSGS1 is required for Arp2/3-dependent actin assembly at the adherens junction. J. Cell Biol. *196*, 115–130.
47. Warren, R.H. (1997). TGF-alpha-induced breakdown of stress fibers and degradation of tropomyosin in NRK cells is blocked by a proteasome inhibitor. Exp. Cell Res. *236*, 294–303.
48. Prasad, G.L., Fuldner, R.A., and Cooper, H.L. (1993). Expression of transduced tropomyosin 1 cDNA suppresses neoplastic growth of cells transformed by the ras oncogene. Proc. Natl. Acad. Sci. USA *90*, 7039–7043.
49. Schevzov, G., Vrhovski, B., Bryce, N.S., Elmir, S., Qiu, M.R., O'Neill, G.M., Yang, N., Verrills, N.M., Kavallaris, M., and Gunning, P.W. (2005). Tissue-specific tropomyosin isoform composition. J. Histochem. Cytochem. *53*, 557–570.
50. Lessard, J.L. (1988). Two monoclonal antibodies to actin: one muscle selective and one generally reactive. Cell Motil. Cytoskeleton *10*, 349–362.
51. Hotulainen, P., and Lappalainen, P. (2006). Stress fibers are generated by two distinct actin assembly mechanisms in motile cells. J. Cell Biol. *173*, 383–394.
52. Comşa, Ş., Cîmpean, A.M., and Raica, M. (2015). The Story of MCF-7 Breast Cancer Cell Line: 40 years of Experience in Research. Anticancer Res. *35*, 3147–3154.
53. Soule, H.D., Maloney, T.M., Wolman, S.R., Peterson, W.D., Jr., Brenz, R., McGrath, C.M., Russo, J., Pauley, R.J., Jones, R.F., and Brooks, S.C. (1990). Isolation and characterization of a spontaneously immortalized human breast epithelial cell line, MCF-10. Cancer Res. *50*, 6075–6086.
54. Dedova, I.V., Dedov, V.N., Nosworthy, N.J., Hambly, B.D., and dos Remedios, C.G. (2002). Cofilin and DNase I affect the conformation of the small domain of actin. Biophys. J. *82*, 3134–3143.
55. Dugina, V., Zwaenepoel, I., Gabbiani, G., Clément, S., and Chaponnier, C. (2009). Beta and gamma-cytoplasmic actins display distinct distribution and functional diversity. J. Cell Sci. *122*, 2980–2988.
56. Gatlin, C.L., Kleemann, G.R., Hays, L.G., Link, A.J., and Yates, J.R., 3rd. (1998). Protein identification at the low femtomole level from silver-stained gels using a new fritless electrospray interface for liquid chromatography-microspray and nanospray mass spectrometry. Anal. Biochem. *263*, 93–101.

STAR★METHODS

KEY RESOURCES TABLE

REAGENT or RESOURCE	SOURCE	IDENTIFIER
Antibodies		
mouse monoclonal anti-γ-actin (clone 2A3)	Biorad	Cat#MCA5776GA; RRID:AB_2571583
sheep polyclonal anti-γ-actin	[49]	N/A
mouse monoclonal anti-actin (clone C4)	[50]	N/A
mouse monoclonal anti-tropomyosin CG3, detecting Tpm3.1-3.11	[22]	N/A
rabbit polyclonal anti-tropomyosin δ/9d, detecting Tpm2.1, Tpm4.1 and Tpm4.2	[22]	N/A
mouse monoclonal anti-tropomyosin Tm311, detecting Tpm1.1-1.7, Tpm1.10, Tpm2.1 and Tpm4.1	Sigma-Aldrich	Cat#T2780; RRID:AB_261632
sheep polyclonal anti-tropomyosin α/1b, detecting Tpm1.8, Tpm1.9, Tpm1.11 and Tpm1.12	[22]	N/A
mouse monoclonal anti-GAPHD (clone 6C5)	Merck	Cat#MAB374; RRID:AB_2107445
mouse monoclonal anti-α-tubulin (clone DM1A)	Sigma-Aldrich	Cat#T9026; RRID:AB_477593
Atto fluor 647N conjugated phalloidin	Atto Tec	Cat#AD 647N-81
Alexa fluor 488 or Alexa Fluor 647 conjugated secondary antibodies	Invitrogen	N/A
HRP conjugated anti-mouse	Abcam	Cat#ab97046
HRP conjugated anti-rabbit	Jackson	Cat#711-035-152
HRP conjugated anti-sheep	Santa Cruz	Cat#SC-2473
Chemicals, Peptides, and Recombinant Proteins		
Latrunculin A	Adipogen	Cat#AG-CN2-0027-C100
MG-132	Sigma-Aldrich	Cat#M7449
Recombinant His-tagged tropomyosins	[22]	N/A
Cholera Toxin	Sigma-Aldrich	Cat#C8052
Insulin	Sigma-Aldrich	Cat#91077C
Hydrocortisone	Sigma-Aldrich	Cat#H0888
Epidermal Growth Factor	Sigma-Aldrich	Cat#E9644
Mowiol 4-88	Sigma-Aldrich	Cat#81381
4 x Laemmli sample buffer	Biorad	Cat#161-0747
Luminata Crescendo Western HRP substrate	Merck	Cat#WBLUR0500
BSA Standard	Pierce	Cat#PI23210
Critical Commercial Assays		
G-actin/F-actin *In Vivo* Assay Biochem Kit	Cytoskeleton, Inc.	Cat#BK037
Precision Red Advanced Protein Assay	Cytoskeleton, Inc.	Cat#ADV02-A
Experimental Models: Cell Lines		
U2OS	[51]	RRID:CVCL_0042
MCF-7	[52]	RRID:CVCL_0031
MCF-10A	[53]	RRID:CVCL_0598
BJpar	[10]	RRID:CVCL_3653
BJeH	[10]	RRID:CVCL_6573
BJeLR	[10]	N/A
Recombinant DNA		
Plasmid: Tpm1.8-NeonGreen	This paper	N/A

(*Continued on next page*)

Continued

REAGENT or RESOURCE	SOURCE	IDENTIFIER
Software and Algorithms		
Excel 2010	Microsoft	https://products.office.com/excel
Prism 7	Graphpad	https://www.graphpad.com/scientific-software/prism/
Fiji (ImageJ)	National Institute of Health, USA	https://fiji.sc/
Mascot v2.5	Matrix Science	http://www.matrixscience.com
Leica Application Suite	Leica	https://www.leica-microsystems.com/products/microscope-software/details/product/leica-application-suite/
Other		
Rabbit skeletal muscle actin	Kindly provided by Irina Dedova [54]	N/A

CONTACT FOR REAGENT AND RESOURCE SHARING

Further information and requests for resources should be directed to and will be fulfilled by the Lead Contact, Prof. Peter Gunning (p.gunning@unsw.edu.au).

EXPERIMENTAL MODEL AND SUBJECT DETAILS

Cell culture

U2OS (Female), MCF-7 (Female), BJpar (Male), BJeH (Male) and BJeLR (Male) cells [10, 51, 52] were cultured in DMEM (Sigma) supplemented with 10% fetal bovine serum (FBS; GIBCO); MCF-10A (Female) cells [53] were cultured in DMEM supplemented with 5% FBS, 0.1 μg/mL Cholera Toxin (Sigma), 10 μg/mL Insulin (Sigma), 0.5 μg/mL Hydrocortisone (Sigma) and 40 ng/mL Epidermal Growth Factor (EGF; Sigma), and kept at 37°C in a humidified chamber with 5% CO2. Cell lines were tested to ensure they were Mycoplasma free.

METHOD DETAILS

Cell transfection

Tpm1.8-NeonGreen plasmid was synthesized by GeneArt in a pcDNA3.1+ expression vector and transfected into cells 48 hr prior to experiment using Lipofectamine3000 (Thermo Fisher) as per manufacturer's instructions.

Immunofluorescence microscopy

Cells were seeded on #1.5 glass 12 mm round coverslips and grown until 90% confluency. Cells were fixed for 30 min in 1% paraformaldehyde (PFA) in DMEM with 20 mM HEPES pre-warmed to 37°C. Coverslips were washed once with PBS before permeabilizing with ice cold methanol for 5 min. Coverslips were washed 6 times with PBS and blocked in 5% (w/v) BSA for 1 hr before proceeding to antibody incubations. Cells to be stained with phalloidin were fixed for 10 min with 4% Paraformaldehyde (PFA) in PBS and permeabilized for 1 hr in 0.1% (v/v) triton-X in 2.5% (w/v) BSA in PBS. Coverslips were washed with PBS before proceeding to the antibody incubations. Antibodies were diluted in 2.5% BSA in PBS and incubated on coverslips for 1 hr at room temperature inside a dark humidified chamber. Coverslips were washed 4 times with PBS between primary and secondary antibody incubations and after secondary antibody incubation, prior to mounting with Mowiol (10% (w/v) Mowiol 4-88 (sigma), 25% (v/v) glycerol, 100mM Tris-HCl pH 8.5). Slides were imaged on a confocal laser scanning microscope (Leica TCS SP5), using a 100x/1.4 oil Plan Apo objective. Images were captured using Leica Application Suite (LAS) acquisition software.

Antibodies and staining

The following primary antibodies were used: mouse monoclonal cytoplasmic γ-actin (Biorad, clone 2A3, 1:250 for IF); sheep polyclonal γ-actin (1:250 for IF); mouse monoclonal C4 actin (1:2000 for western blots); mouse monoclonal CG3 detecting Tpm3.1 and Tpm3.2 (1:250 for IF, 1:500 for western blots); rabbit polyclonal δ/9d detecting Tpm4.1 and Tpm4.2 (1:50 for IF, 1:500 for western blots); mouse monoclonal Tm311 detecting Tpm1.6, Tpm1.7 and Tpm2.1 (Sigma Aldrich, 1:200 for IF, 1:500 for western blots); sheep polyclonal α/1b detecting Tpm1.8 and Tpm1.9 (1:500 for western blots); mouse monoclonal GAPHD (Merck, 1:5000 for western blots); mouse monoclonal α-tubulin DM1A (Sigma, 1:1000 for western blots). All antibodies have been previously described [22, 49, 50, 55].

Secondary antibodies used were raised against the species of the primary antibodies and conjugated with Alexa fluor 488 or Alexa fluor 647 (Invitrogen, 1:500 for IF) or HRP (anti-mouse, Abcam, 1:10,000 for western blots; anti-rabbit, Jackson, 1:5,000 for western

blots; anti-sheep, Santa Cruz, 1:5,000 for western blots). Phalloidin conjugated with Atto fluor 647N (Atto Tec, 1:1000 for IF) was used to stain for F-actin.

Actin and tropomyosin quantification

In order to quantify actin and tropomyosin in cell lysates a set of standards were first prepared. Rabbit skeletal muscle actin was prepared as described in Dedova et al. [54] (Kindly provided by Irina Dedova) and diluted in general actin buffer (5 mM Tris-HCl pH8, 0.2 mM CaCl2, 0.2 mM ATP, 0.5 mM DTT). His-tagged tropomyosins were produced in a pProEXHT vector system and purified as described in Schevzov et al. [22]. Purified actin, tropomyosin and cell lysate total protein concentrations were measured with a Precision Red Advanced Protein assay (Cytoskeleton) using serial dilutions of a BSA standard (Pierce) as a standard curve. For each cell line lysates were collected from 3 different passages by growing cells on 10 cm dishes till 90% confluency, washing once with PBS and harvesting in radio-immunoprecipitation assay buffer (RIPA) (20 mM Tris pH7.4, 150 mM NaCl, 1% (v/v) Nonidet P-40, 0.5% (v/v) sodium deoxycholate, 1mM EDTA, 0.1% (v/v) SDS). Lysates were homogenized via sonication and mixed with appropriate amounts of 4 x Laemmli sample buffer (Biorad) and boiled at 95°C for 10 min. Samples were run on a 10% SDS-PAGE gel and transferred to a PVDF membrane using the Trans-Blot Turbo (Biorad) transfer system, then probed for actin or tropomyosin using specific antibodies. Membranes were developed using Luminata Crescendo Western HRP substrate (Merck) and imaged on a Chemidoc MP imaging system (Biorad), densitometry was quantified in Fiji (downloaded from https://fiji.sc/). Standard curves were plotted in Microsoft Excel and used to calculate the amount of actin or tropomyosin present per known quantity of cell lysate as detailed below.

Let *molTpm* = moles of tropomyosin per gram total protein (see Table 1)
Let *molActin* = moles of actin per gram total protein (see Table 1)
Let grTpm = grams of tropomyosin in lysate
Let grActin = grams of actin in lysate
Let grTotalProtein = grams of total protein in lysate
Let *MWTpm* = Molecular weight of tropomyosin in Da (30,000 Da for Tpm1.8/1.9, Tpm3.1/3.2 & Tpm4.2; 34,000 Da for Tpm1.6/1.7; 38,000 Da for Tpm2.1/4.1 [22])
Let MWActin = Molecular weight of actin in Da (42,000 Da)

$$\text{molTpm} = \frac{\frac{\text{grTpm}}{\text{grTotalProtein}}}{\text{MWTpm}}$$

$$\text{molActin} = \frac{\frac{\text{grActin}}{\text{grTotalProtein}}}{\text{MWActin}}$$

Let *actinperTpm* = the monomeric binding ratio of actin to tropomyosin for a particular tropomyosin isoform, this equals 3 for LMW tropomyosin isoforms (Tpm1.8/1.9, Tpm3.1/3.2 & Tpm4.2) and 3.5 for HMW tropomyosins (Tpm1.6/1.7 & Tpm2.1/4.1).
Let *possible %TpmActin* = % F-actin that could be saturated by tropomyosin (see Table 1)

$$\text{Let i} = \{\text{Tpm1.6/1.7},\ \ \text{Tpm1.8/1.9},\ \ \text{Tpm2.1/4.1},\ \ \text{Tpm3.1/3.2},\ \ \text{Tpm4.2}\}$$

$$\text{possible } \%\text{TpmActin} = \left(\frac{\sum^{i}(\text{molTpm} \times \text{actinperTpm})}{\text{molActin} \times \text{fActin}}\right) \times 100\%$$

Let [Tpm] = the estimated molar concentration of tropomyosin in a cell (See Table S1)

$$\text{Let the concentration of total protein in the cell} = \frac{200\text{g}}{\text{L}}$$

[30, 31]

$$[\text{Tpm}] = \left(\text{molTpm} \times \frac{200\text{g}}{\text{L}}\right)$$

Let $K_{d(app)}$ = the experimental equilibrium constant indicating the concentration of tropomyosin required to saturate 50% of actin filaments (See Table S2 or [4, 32])
Let n = the experimentally determined Hill coefficients (See Table S2 or [4, 32])
Let *%TpmBindingPrediction* = % Tropomyosin predicted to bind actin filaments based on Hill Equation [4] (see Table S2)

$$\%\text{TpmBindingPrediction} = \left(\frac{[\text{Tpm}]^n}{K_{d(app)} + [\text{Tpm}]^n}\right) \times 100\%$$

Let *fTpm* = fraction of tropomyosin in pellet (See Figure 2G)
Let *fActin* = fraction of actin in the form of F-actin (See Figure 2G and Table 1)
Let *%TpmActin* = The % F-actin that is associated with tropomyosin (see Figure 2H)

$$\%\text{TpmActin} = \left(\frac{\sum^i(\text{molTpm} \times \text{fTpm} \times \text{actinperTpm})}{\text{molActin} \times \text{fActin}}\right) \times 100\%$$

Let *SDmolTpm* = standard deviation of moles of tropomyosin per gram total protein
Let *SDfTpm* = standard deviation of fraction of tropomyosin in pellet
Let *%Error TpmActin* = % error of F-actin associated with tropomyosin (see Figure 2H)

$$\%\text{Error TpmActin} = \left(\frac{\sum^i\left(\sqrt{(\text{SDfTpm} \times \text{molTpm})^2 + (\text{SDmolTpm} \times \text{fTpm})^2} \times \text{actinperTpm}\right)}{\text{molActin} \times \text{fActin}}\right) \times 100\%$$

Tropomyosin partitioning assay

Cells were plated on 10cm dishes and grown till 90% confluency. Cells were washed twice with 37°C PBS before harvesting in 500 μL LAS2 lysis and F-actin stabilization buffer prepared as per manufacturer's instructions and pre-warmed to 37°C, from the G-actin/F-actin *In Vivo* Assay Biochem Kit (Cytoskeleton). Samples were further processed using the G-actin/F-actin *In Vivo* Assay Biochem Kit (Cytoskeleton) as per manufacturer's instructions. Briefly, lysates were transferred to a pre-warmed Eppendorf tube and homogenized by pipetting up and down 10 times, then incubated at 37°C for 20 min (beginning after cell suspension in LAS2). Unbroken cells were pelleted by centrifuging lysates at 2000rpm for 5 min in an Eppendorf 5415R tabletop centrifuge pre-warmed to 37°C, supernatant was then collected in a pre-warmed Eppendorf tube labeled 'total lysate'. 200 μL of total lysate was transferred into a pre-warmed ultracentrifuge tube (Hitachi, 0.5PC, S300533A) and centrifuged at 100,000 x g for 1 hr at 37°C in a Hitachi CS150NX tabletop micro ultracentrifuge fitted with a S120AT3 rotor. After centrifugation, the supernatant (G-actin) was immediately transferred into an Eppendorf tube labeled 'G-actin supernatant' and placed on ice. The F-actin pellet was resuspended in 200 μL F-actin depolymerization solution (Cytoskeleton) transferred into a tube labeled 'F-actin pellet' and incubated on ice for 1 hr, vortexing every 15 min. Samples were mixed with an appropriate amount of 4 x Laemmli sample buffer (Biorad) and the G-actin sample was boiled at 95°C for 10 min. The F-actin sample was not boiled due to the urea in the F-actin depolymerization solution, but instead incubated at 37°C for 10 min prior to loading the sample on a gel. Equal volumes were run on a 10% SDS-PAGE gel, transferred to a PVDF membrane, probed with specific anti-actin and tropomyosin antibodies and developed as before. Densitometry and ratios were analyzed using Fiji and Excel.

Liquid chromatography (LC)

Nano-Liquid chromatography (nano-LC) was performed using an Ultimate 3000 HPLC and autosampler system (Dionex, Amsterdam, Netherlands). Samples were injected into a fritless nanoLC column (75 μm x ~12 cm) containing C18 media (1.9μm, 120 Å ReproSil-Pur 120 C18-AQ, Dr Maisch GmbH) manufactured according to Gatlin [56] and heated to 45°C for all runs. Peptides were eluted using a linear gradient according to the conditions in the table below, over 52 min, at a flow rate of 0.200 μL/min. Mobile phase A consisted of 0.1% Formic Acid in H2O, while mobile phase B consisted of ACN:H2O (8:2) with 0.1% Formic Acid.

Liquid chromatography conditions for peptide separation prior to MS/MS

Time (min)	%B
0.0	2.0
4.0	2.0
36.0	45.0
37.0	80.0
37.5	80.0
39.0	2.0
52.0	2.0

Tandem mass spectrometry (MS/MS)

High voltage (2000 V) was applied to a low volume tee (Upchurch Scientific) and the column tip positioned ~0.5 cm from the heated capillary (T = 275°C) of a LTQ Orbitrap Velos (Thermo Fisher Scientific, Waltham, Massachusetts, USA) mass spectrometer. Positive ions were generated by electrospray and the mass spectrometer operated in data dependent acquisition mode (DDA). Full scan MS spectra were acquired (m/z 350-1750) by the Orbitrap at a resolution of 30,000. The 15 most abundant ions (> 5,000 counts) with charge states $\geq$ +2 were sequentially isolated and fragmented within the linear ion trap using collisionally induced dissociation with an activation q = 0.25 and activation time of 10 ms at a target value of 30,000 ions. M/z ratios selected for MS/MS were dynamically excluded for 35 s.

Peak lists of MS/MS data were generated using Mascot Daemon/extract_msn (Matrix Science, London, England) and were entered into the search program Mascot version 2.5 (http://www.matrixscience.com) and searched against *Homo sapiens* proteins in the NCBIprot database in March 2017. Precursor tolerances were 4 ppm and product ion tolerances were ± 0.4 Da. Modifications accounted for are Carbamidomethyl (C), Oxidation (M), Propionamide (C) and Acetyl (N-term) with trypsin and 1 missed cleavage was possible. No decoy database was employed.

Drug treatments

For all of the drug assays cells were grown to 90% confluency in 10 cm dishes. Drugs were diluted in growth media, Lat A (Adipogen) was used at 1 μM unless specified otherwise, MG132 (Sigma) was used at 20 μM and DMSO volume was equalised across treatment groups.

QUANTIFICATION AND STATISTICAL ANALYSIS

All values in the text are presented as mean ± standard deviation and number of experimental replicates is indicated in the figure legends. Data were analyzed in Microsoft Excel 2010 and two-sample two-tailed t tests were used to compare treatment groups with DMSO control. All graphs were produced using Prism (Graphpad Software).